Clinical Neurophysiology 130 (2019) 1628–1641

Contents lists available at ScienceDirect

Clinical Neurophysiology

journal homepage: www.elsevier.com/locate/clinph

The seizure onset zone drives state-dependent epileptiform activity in susceptible brain regions

Joshua M. Diamond [a], Julio I. Chapeton [a], William H. Theodore [b], Sara K. Inati [c,*], Kareem A. Zaghloul [a,*]

[a] Surgical Neurology Branch, NINDS, National Institutes of Health, Bethesda, MD 20892, United States
[b] Clinical Epilepsy Section, NINDS, National Institutes of Health, Bethesda, MD 20892, United States
[c] Epilepsy Service and EEG Section, NINDS, National Institutes of Health, Bethesda, MD 20892, United States

ARTICLE INFO

Article history:
Accepted 14 May 2019
Available online 2 July 2019

Keywords:
Interictal epileptiform discharges
Epilepsy networks
Sleep
Intracranial EEG

HIGHLIGHTS

- Interictal epileptiform discharges (IEDs) may be grouped using community detection.
- The seizure onset zone (SOZ) often leads IED activity within cortical communities.
- Spread of IEDs from the SOZ to surrounding tissues is enhanced in the asleep state.

ABSTRACT

Objective: Due to variability in the patterns of propagation of interictal epileptiform discharges (IEDs), qualitative definition of the irritative zone has been challenging. Here, we introduce a quantitative approach toward exploration of the dynamics of IED propagation within the irritative zone.
Methods: We examined intracranial EEG (iEEG) in nine participants undergoing invasive monitoring for seizure localization. We used an automated IED detector and a community detection algorithm to identify populations of electrodes exhibiting IED activity that co-occur in time, and to group these electrodes into communities.
Results: Within our algorithmically-identified communities, IED activity in the seizure onset zone (SOZ) tended to lead IED activity in other functionally coupled brain regions. The tendency of pathological activity to arise in the SOZ, and to spread to non-SOZ tissues, was greater in the asleep state.
Conclusions: IED activity, and, by extension, the variability observed between the asleep and awake states, is propagated from a core seizure focus to nearby less pathological brain regions.
Significance: Using an unsupervised, computational approach, we show that the spread of IED activity through the epilepsy network varies with physiologic state.

1. Introduction

Interictal epileptiform discharges (IEDs) are an electrographic manifestation of excessive hypersynchronization of cortical activity, and are considered to be biomarkers of potentially epileptogenic tissue (de Curtis and Avanzini, 2001). The brain regions generating IEDs, collectively referred to as the irritative zone, usually overlap with the areas of the brain generating seizures, but this relationship is not always straightforward. Although the irritative zone is often described as a distinct entity, it exhibits significant spatial and temporal variability, making its analysis complementary to, yet distinct from, investigations of the seizure onset zone (SOZ).

Spatially, the irritative zone can be focal, but may also extend across larger brain regions and include multiple presumably independent subnetworks, each with its own independent populations or communities of IEDs (de Curtis and Avanzini, 2001; Luders et al., 2006). Within a given IED community, there tends to be a consistent spatial core of activity. However, variability in IED frequency in the brain regions within a given community may increase with increasing distance from the spatial core, as well as with changes in local and global brain states such as state of arousal (de Curtis and Avanzini, 2001; Sabolek et al., 2012; Janca et al., 2018;

* Corresponding authors at: Surgical Neurology Branch, NINDS, National Institutes of Health, Building 10, Room 3D20, 10 Center Drive Bethesda, MD 20892-1414, United States (K.A. Zaghloul); Office of the Clinical Director, NINDS, National Institutes of Health, Building 10, Room 7-5680, 10 Center Drive Bethesda, MD 20892-1445, United States (S.K. Inati).
E-mail addresses: sara.inati@nih.gov (S.K. Inati), kareem.zaghloul@nih.gov (K.A. Zaghloul).

https://doi.org/10.1016/j.clinph.2019.05.032
1388-2457/Published by Elsevier B.V. on behalf of International Federation of Clinical Neurophysiology.

Sammaritano et al., 1991; Malow et al., 1999; Alarcon et al., 1994; Emerson et al., 1995). This is generally understood to represent state-dependent propagation of pathological activity from more epileptogenic source regions to functionally connected, less pathological cortical regions (Goncharova et al., 2013).

Temporally, long-term intracranial EEG (iEEG) recordings have demonstrated fairly reproducible circadian and multidien fluctuations in both IEDs and seizure activity within individual patients (Baud et al., 2018; Karoly et al., 2016), but additional variability can emerge due to local metabolic and neuromodulatory factors operating at the neuronal level (Jirsa et al., 2014). Although it is difficult to measure or control many of these potential influences on brain state, state of arousal is a factor that is easily observable and has been shown to affect both seizures and IEDs. Increased rates of IED activity have been observed during NREM sleep, due at least in part to increased synchronization (Sammaritano et al., 1991; Malow et al., 1999; Steriade et al., 1994).

This spatial and temporal variability has made precise characterization of reproducible patterns within the irritative zone challenging, and indeed, grouping IEDs through visual inspection into a core set of electrodes that define a community is largely a probabilistic estimation. Several quantitative approaches have been developed that have improved our understanding of these local interactions within the irritative zone. Automated extraction techniques have identified subsets of brain structures frequently and conjointly involved in the generation of IEDs (Bourien et al., 2005; Wendling et al., 2009). Investigation of propagation patterns within communities have shown that leading regions are highly correlated with the eventual site of seizure origin (Hufnagel et al., 2000; Asano et al., 2003; Alarcon et al., 1997; Tomlinson et al., 2016). And network-based approaches have identified increased connectivity within the epileptogenic zone both during and between seizures (Varotto et al., 2012; Wilke et al., 2011; Van Mierlo et al., 2011; Lopes et al., 2017; Chiang and Haneef, 2014).

Here, we describe an automated probabilistic method of generating communities of IED activity based on the co-occurrence of IEDs within the irritative zone in participants with focal epilepsy. We show that examining such conditional co-occurrences of IEDs within these communities provides valuable insight into the dynamics within the irritative zone. Consistent with previous work, we show that the SOZ drives pathological IED activity in functionally coupled surrounding brain regions. Both initiation and propagation of IED activity are enhanced in the asleep state, leading to a robust increase in IED activity during this state at the community level.

2. Materials and methods

2.1. Study participants and recordings

Nine participants who underwent surgical placement of subdural and depth electrodes for intracranial seizure monitoring participated in this study. Patient demographic and clinical information is provided in Table 1. Surgical procedures and video-EEG monitoring were performed at the Clinical Center at the National Institutes of Health (NIH; Bethesda, MD). The research protocol was approved by the Institutional Review Board, and informed consent was obtained from all participants. We analyzed all data using custom Matlab scripts (Mathworks, Natick, MA). We provide descriptive statistics as mean ± standard deviation (SD) unless otherwise stated. All reported *p*-values are two-sided.

We recorded continuous intracranial EEG (iEEG) data from subdural contacts (PMT Corporation, Chanhassen, MN) sampled at 1000 Hz using a Nihon Kohden EEG data acquisition system. Subdural contacts were arranged in both grid and strip configurations with an inter-contact spacing of 10 mm. We manually rejected electrodes exhibiting obvious artifacts, abnormal signal amplitude, or large line noise. For each electrode, we applied a local detrending procedure to remove slow fluctuations from the time series and used a regression-based approach to remove line noise at 60 Hz and 120 Hz (Mitra, 2007). We used a low-pass type I FIR filter (order = 110, fcutoff = 165 Hz) to remove higher order line harmonics as well as high frequency noise (Chapeton et al., 2017). We localized electrodes in each participant by co-registering the postoperative CTs and mapped these locations to both MNI and Talairach space (Trotta et al., 2017). Preoperative MRIs were used when postoperative MRIs were not available. Each electrode was assigned a three-dimensional coordinate in each participant's own anatomic space based on localization, and pairwise distances between electrodes were computed by taking the Euclidian distance between coordinates.

We captured iEEG data during the entirety of each participant's stay in the Epilepsy Monitoring Unit. Continuous data were divided into two-hour epochs by the data acquisition system. All epochs selected for our analysis were separated by at least 24 h from a seizure event, to account for the fact that IED rates may be elevated following seizure (Gotman and Marciani, 1985). Awake and asleep epochs were chosen based on video monitoring data. During asleep epochs, the participant was lying quietly with closed eyes and exhibited minimal body movement and regular respiration for the duration of the epoch. During awake epochs, the participant

Table 1
Patient characteristics.

Patient	Sex	Age at seizure onset	Age at surgery	Seizure type(s)	MRI	Scalp EEG findings	Procedure	Pathology	Seizure outcome (engel class)	Months follow up
1	F	14	30	SPS, CPS, rare 2GTCS	NL	L FT	L SAH	HS, MDG	2b	27
2	F	4	49	SPS, CPS, rare 2GTCS	L MTS	B T	L SAH	HS	3a	24
3	F	19	35	CPS, 2GTCS	possible b/l MTS	B FT	R ATL	HS, MDG	1a	30
4	M	40	51	CPS, 2GTCS	LF SDH	L FT	L SAH	gliosis	UNK	0
5	F	41	58	CPS, 2GTCS	NL	L>R FT	L ATL	HS, MDG	1a	3
6	F	19	28	CPS	possible L MTS	L T	L ATL	HS, MDG	1a	24
7	F	13	30	CPS	R parietal encephalo-malacia, possible R MTS	R>L FT	R ATL	HS	1b	24
8	M	3	34	2GTC	NL	Multifocal	R parietal topectomy	MDG	2b	24
9	M	12	18	CPS	NL	L parasagittal	No resection	N/A	N/A	N/A

SPS: simple partial seizures. CPS: complex partial seizures. 2GTCS: secondarily-generalized tonic-clonic seizures. NL: non-localizing. SAH: selective amygdalohippocampectomy. ATL: anterior temporal lobectomy. MTS: mesial temporal sclerosis. Possible MTS: subtle FLAIR hyperintensity, relatively preserved structure. SDH: subdural hematoma. FT: frontotemporal. HS: Hippocampal sclerosis. MDG: microdysgenesis. UNK: unknown (patient lost to follow up).

was carrying out spontaneous activities with eyes open for the duration of the epoch.

A board-certified epileptologist experienced in the clinical review of intracranial EEG, and blinded to our analysis, identified the individual electrodes that were involved in the first several seconds of seizure onset during any seizure recorded over the entire monitoring period (Marsh et al., 2010; Wang et al., 2013). Importantly, only ictal data was used for this designation. These electrodes were designated seizure onset zone (SOZ) electrodes.

2.2. Automated IED detection

We used an automated IED detector, written in custom scripts, in order to identify IED events. Our IED detector works similarly to IED detectors which have been created and validated in previous work (Brown et al., 2007; Gaspard et al., 2014). The automated IED detector took raw iEEG time series data as input (Fig. 1a). For each two-hour epoch of recorded data, we computed the mean, μ, and standard deviation, σ, of the iEEG trace separately for each electrode. We defined peaks and troughs in the raw iEEG trace as those time points during which the iEEG recorded signal was greater than $\mu + 3\sigma$ or less than $\mu - 3\sigma$, respectively. We defined each IED event as those instances where both a peak and a trough occurred within a single 100 ms window, and where the peak-trough height was greater than or equal to 9σ. Additionally, either the peak, trough, or both must have had a topographic prominence of 3σ, within the defined 100 ms window.

Detected IEDs may either have a morphology in which a peak precedes the trough or one in which a trough precedes a peak. Either the peak or the trough, or both, may meet the prominence requirement. This therefore results in four total morphologies, which are not mutually exclusive. A set of example IEDs with one such morphology is shown in Fig. 1b. After we identified all IEDs for a given electrode in a given epoch, we selected the preferred morphology for IED events for that electrode. We defined the preferred morphology as that for which a threshold IED rate was exceeded (0.025 IEDs/min) and for which the peak-to-trough distance of the mean trace was the largest among all morphologies which met the threshold requirement. In practice, however, the identity of the preferred morphology was usually obvious on visual inspection of the extracted waveforms, in that, for the preferred morphology, these waveforms were more numerous, had greater peak-trough height, and more closely resembled typical IEDs. Indeed, IED morphology tended to be relatively uniform within individual electrodes. Once we identified the preferred morphology for a given electrode, we recorded the times during which IED events of that morphology occurred for further analysis (Fig. 1c). In each participant, we used our automated IED detector to create a pool of all electrodes which exhibit IED activity.

A board-certified epileptologist experienced in the clinical review of intracranial EEG reviewed the recordings for each participant blinded to our analysis and identified individual IEDs, so as to validate our IED detector. We randomly selected a single epoch from each of three participants for validation. Within each of these epochs, we then randomly selected three electrodes, yielding a total of nine electrodes with detected IED activity that we compared to the clinically-identified events. Our detection algorithm identified IED events with a sensitivity of 0.64, a positive predictive value (PPV) of 0.69, and a false detection rate of 1.39 per minute. This performance is similar to or better than that of previously

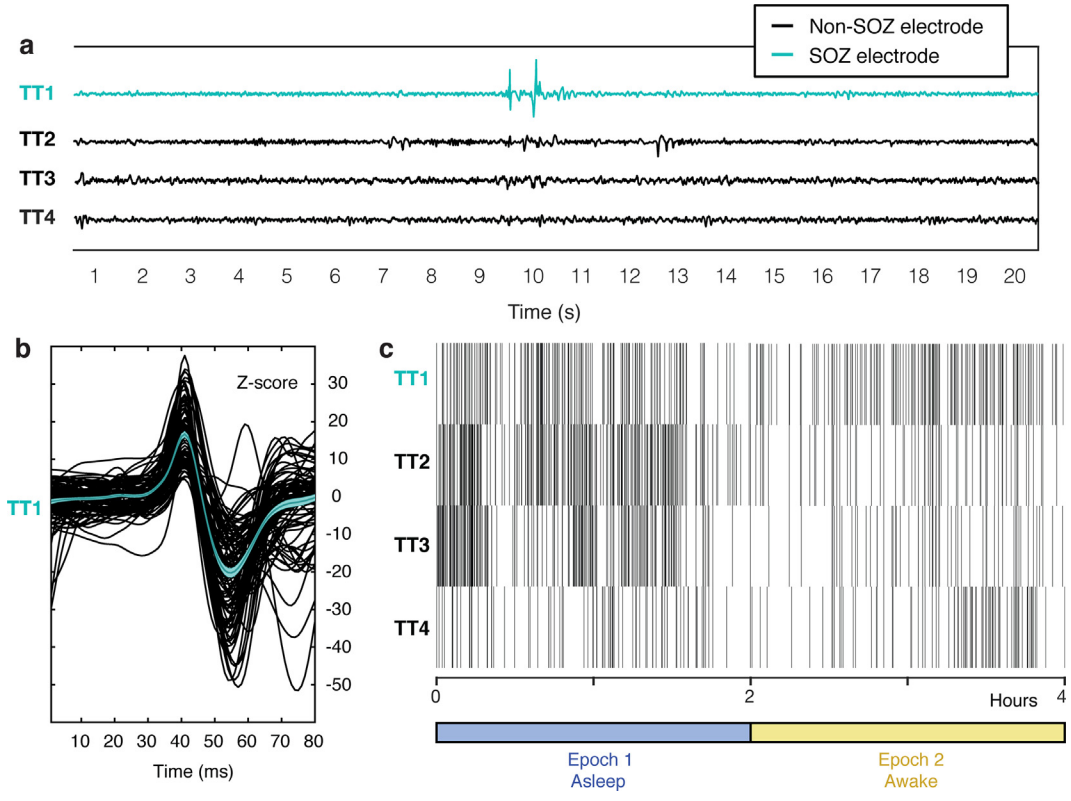

Fig. 1. Automated IED detection. **(a)** Raw iEEG traces from four intracranial electrodes in a single participant, characterized by the presence of IEDs. Independent from our analysis, a clinical epileptologist identified electrodes involved in the seizure onset zone (SOZ, teal). Remaining electrodes were designated as non-SOZ (*black*). **(b)** The automated IED detection algorithm searched for large fluctuations in the amplitude of the voltage time series (see Section 2.2, Automated IED detection). All waveforms of a single IED morphology (*black*), in a single electrode and epoch, and the average across all IEDs in this electrode (*teal*) are shown. **(c)** The time of each IED is recorded for each electrode and retained for further analysis. The raster plot for the four representative electrodes from **a** is shown throughout a single awake and asleep epoch. (For interpretation of the references to colour in this figure legend, the reader is referred to the web version of this article.)

described automated IED detectors (Brown et al., 2007; Gaspard et al., 2014). Of note, accurate IED detection remains a challenge, as even agreement between clinical epileptologists on IED classification may be as low as 41% (Gaspard et al., 2014). We found that the sensitivity of our IED detection algorithm increased, and the PPV decreased, as we decreased the threshold criterion for IED amplitude, but both were generally robust to parameter changes.

2.3. IED coupling between electrodes

In order to determine whether a pair of electrodes are coupled, we computed the conditional probability that an IED event in one electrode would occur given that an IED event occurred in another. We defined S_i and S_j as a binary metric of whether or not an IED was observed in electrodes e_i and e_j, respectively, at a given time. We defined the instances in which an IED in electrode e_i leads an IED in electrode e_j as S_i, S_j, and imposed three constraints on such instances. First, if electrodes e_i, e_j, and e_k participated in a sequence of IED events, in that order, we only considered co-occurrences with the leader electrode $e_i : S_i, S_j$ and S_i, S_k, but not S_j, S_k. Second, to consider only electrode pairs in which an IED event in one leads an IED in another, we only retained instances of S_i that occur no more than 50 ms before S_j (Alarcon et al., 1997; Tomlinson et al., 2016). Finally, to eliminate any possibility that the coordinated IED events we observe might arise from volume conduction, we only considered instances of S_i that occur at least 1 ms prior to S_j. Three example electrodes exhibiting IEDs, and the time relation between them, are depicted in Fig. 2a.

We used such instances of S_i, S_j to compute the conditional probability, $P(S_i|S_j)$, which describes the likelihood that an IED in e_i was present immediately before an IED was present in e_j. We computed $P(S_i|S_j)$ by dividing the probability of observing an instance of S_i, S_j by the probability of observing an IED in e_j:

$$P(S_i|S_j) = \frac{P(S_i, S_j)}{P(S_j)}$$

We designated e_i and e_j as *coupled* if IEDs identified in electrode e_i consistently led IEDs identified in electrode e_j (high value of $P(S_i|S_j)$), if e_j consistently led e_i (high value of $P(S_j|S_i)$), or both. For the case $i = j$, we defined $P(S_i|S_j)$ as 0. Note that, rather than using the joint probability $P(S_i, S_j)$, we used a conditional probability in which we normalized the joint probability to the IED rate of the follower electrode, so that two electrodes that simply have a high rate of IED activity are not coupled unless the IED activity of one is dependent upon the other. In this manner, we established a probabilistic measure of the extent to which IED activity in the follower electrode depends on the IED activity in the leader to spike. Hence, if $P(S_i|S_j)$ is high, e_i led nearly every time electrode e_j had an IED event, and therefore e_j usually cannot independently exhibit an IED without e_i. It may still be the case, though, that e_i often exhibits IEDs without giving rise to an IED in e_j. Thus, for any two electrode contacts, we can assess a bidirectional measure of dependence.

2.4. Automated community detection

We used the conditional probabilities of IED events between electrodes to construct a weighted adjacency matrix, w, where each element w_{ij} of the adjacency matrix represents the coupling, given by the conditional probability, between every pair of electrodes e_i and e_j:

$$w_{ij} = P(S_i|S_j)$$

The adjacency matrix, w, thus provides the edge weights of a directed graph. w is not symmetric, as IED activity in one electrode may drive, yet occur independently of, activity in another. w for one representative participant is shown in Fig. 2b. To group electrodes with co-occurring IEDs into communities, we used the spectral optimization technique for community detection (Newman, 2006), generalized to accept directed graphs (Leicht and Newman, 2008). This algorithm was implemented in the Brain Connectivity Toolbox (Rubinov and Sporns, 2010).

Beyond simply detecting groups of electrodes with disproportionately high coupling between them, we sought to also account for the fact that electrodes which are closer to each other may be more likely to have high coupling strength simply by virtue of their distance. To address this, we implemented the *gravity* constraint (Expert et al., 2011). This method uses the empiric adjacency matrix to create a deterrence function, which effectively penalizes electrodes which are close and rewards electrodes which are far away. This deterrence function is affixed to the null model.

We started with a null model which resembles the Newman-Girvan model (Newman and Girvan, 2004), modified for directed graphs (Leicht and Newman, 2008):

$$P_{ij} = k_i^{in} k_j^{out}$$

We then modified the null model further by adding the deterrence function f (Expert et al., 2011):

$$P_{ij} = k_i^{in} k_j^{out} f(d_{ij})$$

where the deterrence function $f(d)$ is given by

$$f(d) = \frac{\sum_{i,j|d_{ij}=d} w_{ij}}{\sum_{i,j|d_{ij}=d} k_i^{in} k_j^{out}}.$$

$f(d)$ gives greater weight to the elements of the null model if, simply because those electrodes are located close in space, those elements have a stonger connection strength. Note that the total weight of the null network P is equal to that of w.

Since the set of possible distances d_{ij} is continuous, we implemented a binning scheme to discretize these values. We separated the set of all distances into bins of 200 elements each, such that there were usually between 20 and 30 bins. We considered several binning methods, including choosing bins of equal element count or bins of equal distance (explored in Sarzynska et al., 2015). The choice of binning paradigm did not have a significant effect on our results. Note that the deterrence function, as originally described, was intended for undirected graphs (Expert et al., 2011). This method easily generalizes to directed graphs. In computing $f(d)$, for two electrodes e_i and e_j separated by some distance d, we simply include the respective cell in both the upper and lower triangles of the adjacency matrix w, and of the node importance matrix $k_i^{in} k_j^{out}$, as summands in the numerator and denominator, respectively, of the expression for $f(d)$.

Using our null model, we then proceeded with modularity maximization (Leicht and Newman, 2008). Here, the modularity Q is maximized, with Q given by

$$Q = \frac{1}{m} \sum_{ij} [w_{ij} - \gamma \cdot P_{ij}] \delta_{c_i,c_j}.$$

γ is a resolution parameter which allows for control of the community size. A larger value of γ gives greater weight to the null model, and therefore promotes the selection of smaller communities. We used $\gamma = 1$ as our resolution parameter, which has been used canonically. δ_{ij} is the Kronecker delta symbol, and c_i reflects the community assignment of electrode e_i. Thus, multiplication by δ_{c_i,c_j} restricts computations of modularity only to connection strengths within each community. m represents the summed weight of all edges in w.

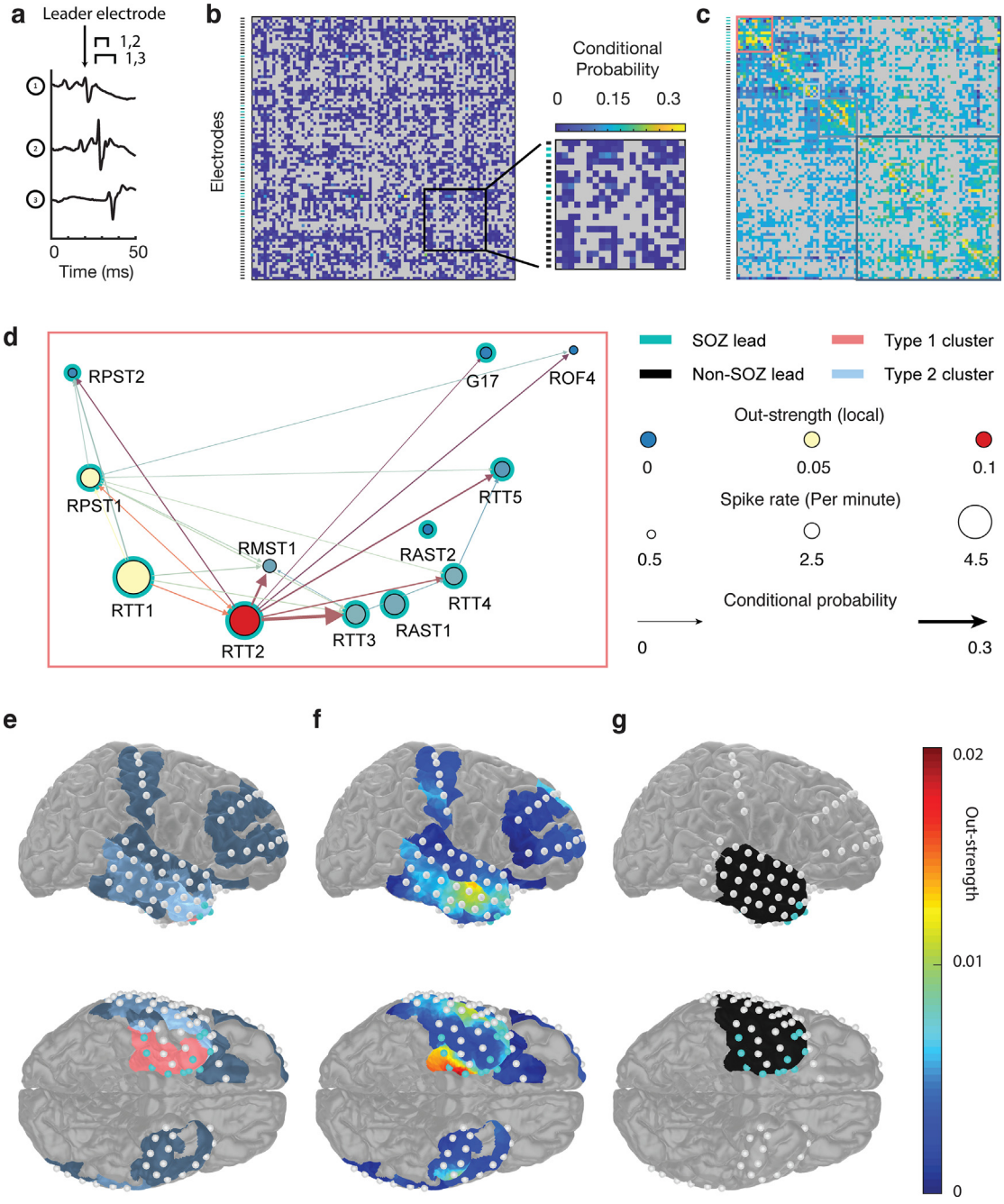

Fig. 2. Automated community detection. **(a)** To determine if two electrodes were coupled, we identified all instances in which IEDs occurred in two or more electrodes within the same 50 ms window. **(b)** These IED co-occurrences were used to calculate the conditional probability that, when an IED was present in one electrode, the other electrode led the IED sequence. These conditional probabilities were used to populate the weighted directed adjacency matrix *w*, shown in panel **b**, and served as a measure of directed coupling strength between every electrode pair. The inset demonstrates a close up view of the adjacency matrix. **(c)** We created the *modularity matrix* by starting with the empiric matrix (**b**) and adjusting each coupling strength for node degree and spatial spread (see Methods). This modularity matrix was then put into our community detection algorithm, which groups electrodes into communities such that these adjusted coupling strengths are disproportionately-high within communities. The output is shown in (**c**). Using a permutation test, we identified those communities that were unlikely to have arisen by chance. These were labelled as Type 1 communities if they contained 10% or greater SOZ electrodes (shades of *red*), or Type 2 communities if they contained fewer than 10% SOZ electrodes (shades of *blue*). **(d)** This diagram provides an illustration of the network behavior of this patient's sole Type 1 community (shown in panel **c**, top left). Electrode size corresponds to IED rate. Electrode color corresponds to the electrode's out-strength, which is a measure of the electrode's cumulative tendency to lead other electrodes within its community. Arrow size represents coupling strength, and arrow color reflects the average between source and destination node out-strength. Electrodes encircled in *teal* are SOZ electrodes. The SOZ electrodes tend to have the greatest out-strength. Coupling relationships are dynamic: the electrode with the greatest out-strength is at times led by other electrodes, and other electrodes with lesser overall out-strength have similar spiking rate. RTT: right temporal tip; RAST: right anterior subtemporal; RPST: right posterior subtemporal; ROF: right orbitofrontal; RAST: right anterior subtemporal; G: grid. **(e–g)** Cortical surface reconstruction of this participant demonstrating the anatomic location of every electrode; right lateral view (top) and inferior view (bottom). Electrodes shown in teal are the clinically-identified SOZ electrodes. **(e)** Algorithmically-identified IED communities within this patient. Colors match those used in **c**; shades of *red* indicate Type 1 communities, while shades of *blue* indicate Type 2 communities. **(f)** Heatmap indicating the global out-strength of each electrode. As in **d**, we see that the greatest out-strength is seen in the mesial temporal region within the SOZ. **(g)** The resection territory for this particular patient is shown in black. The resection territory encompasses this patient's sole Type 1 cluster, as well as elements of several Type 2 clusters (panel **f**). The resection territory also contains those electrodes with greatest out-strength (panel **f**). This patient experienced seizure freedom following resection. (For interpretation of the references to colour in this figure legend, the reader is referred to the web version of this article.)

The modularity Q is maximized when each community has strong connections between its members and relatively weaker connections with nodes outside the community. The community organization of the modularity matrix $[w_{ij} - \gamma \cdot P_{ij}]$ in a particular participant is shown in Fig. 2c. Note that all electrodes are placed into communities, even though the modularity of some communities may not be particularly high. To address this, we used a permutation test to identify those communities with statistically-significant modularity. This permutation test was implemented in the Network Community Toolbox. For each participant, we permuted the community assignments for each node, e_i, 1000 times. Note that, after each permutation, each community still contained the same number of nodes. We then reassessed the modularity of each individual community. Thus, for each community, we obtained 1000 modularity values, each corresponding to a random reassignment of node members. From these modularity values, we obtained the mean and standard deviation, and took the z-score of the true modularity value. We designated communities with $z > 6$ as significant. We chose the threshold $z = 6$ because substantially lower threshold values were insufficient to result in a significant reduction of our community count. However, our results were generally robust to changes in the z-score threshold.

We were interested in comparing those communities which contained drivers of pathological activity to those which did not. Therefore, we designated our algorithmically-identified communities as Type 1 and Type 2 communities, as follows: if at least 10% of electrodes within an identified community were SOZ electrodes, we defined that community as a Type 1 community. On the other hand, if fewer than 10% of electrodes within a given community were SOZ electrodes, we defined it as a Type 2 community. Thus, Type 1 communities contained SOZ and non-SOZ electrodes, while Type 2 communities contained few, or, more often, no SOZ electrodes.

Before the permutation procedure, we identified 46 communities across all participants, comprising 727 electrodes, of which 74 were SOZ. Mean pairwise distance between electrodes in these communities was 4.23 ± 1.96 cm. Each patient had median 5 (range 3–7) communities, of which median 1 (range 0–4) were Type 1. After the permutation procedure, we retained 33 communities across all participants, comprising 583 electrodes, of which 57 were SOZ. Mean pairwise distance was 4.49 ± 2.02 cm. Because the community detection procedure measures modularity in a space-independent fashion (Expert et al., 2011), the community spatial spread was not expected to change after the permutation procedure. After the permutation procedure, each participant had median 4 (range 1–6) communities, of which median 1 (range 0–3) were Type 1.

2.5. Electrode leading and susceptibility

The adjacency matrix w reflects the extent to which each electrode leads or is led by other electrodes. Given a single participant with n total electrodes, if w_{ij} is high for some i and all $j \in \{1, \ldots, n\}$, then electrode e_i on average leads the other n electrodes. Likewise, if w_{ji} is high for some i and all $j \in \{1, \ldots, n\}$, then we may infer that electrode e_i is led, on average, by the other n electrodes. We therefore established measures of whether a given electrode, e_i, on average, leads or is led by other electrodes in the global network, as the *global* out-strength, $s_{\text{out}}(e_i)$ and in-strength, $s_{\text{in}}(e_i)$ respectively:

$$s_{\text{out}}(e_i) = \frac{1}{n}\sum_{j=1}^{n} w_{ij}$$

$$s_{\text{in}}(e_i) = \frac{1}{n}\sum_{j=1}^{n} w_{ji}$$

These measures simply take the mean of the outward and inward coupling strengths, respectively, for a particular electrode e_i. Out-strength and in-strength have been previously used in graph theory to capture asymmetric control and influence relationships (Barrat et al., 2007; Opsahl et al., 2010; Newman, 2001). With these metrics, we may quantify coupling of IED activity more explicitly than do previous studies that considered leading electrodes in IED sequences (Alarcon et al., 1997; Hufnagel et al., 2000). IED behavior is often highly variable, likely due in part to the fact that IED activity is subject to both local and network influences (Karoly et al., 2016; Baud et al., 2018; Jirsa et al., 2014). Our probabilistic approach may be better suited than previous methods to capture IED leading and entrainment relationships in the setting of this variability.

The out-strength and in-strength may be defined by using all electrodes in a given participant, or by using only the electrodes within a given community. Further, we may or may not choose to restrict computations of strength to a subset of electrode relationships, such as those between SOZ and non-SOZ electrodes.

For some community C and electrode $e_i \in C$, we can compute the *local* out-strength, as follows:

$$s_{\text{out}}(e_i \in C) = \frac{1}{|C|}\sum_{e_j \in C} w_{ij}$$

where $|C|$ denotes the number of electrodes in the set C. Local in-strength is computed similarly (see the equation for global in-strength). Note that we only examine local out-strength and local in-strength for electrodes within communities which were deemed significant after our permutation test.

We can also compute the extent to which an electrode's IED activity affects IEDs in electrodes that lie outside of its community. We designate this as that electrode's *external* out-strength:

$$s_{\text{out}}(e_i \in C) = \frac{1}{|\{e_j \notin C\}|}\sum_{e_j \notin C} w_{ij}$$

which captures how much IED activity in a given electrode e_i drives IEDs in all other electrodes that are not in e_i's community.

We may also compute the local in- or out-strength by only considering the relationships across electrode SOZ types. We denote Z as the set of electrodes in a particular participant that are SOZ. Thus, $e_i \in C \cap Z$ denotes an electrode in community C that is also an SOZ electrode, and $e_i \in C \setminus Z$ denotes an electrode in community C which is not SOZ. The *modified* local out-strength for some electrode $e_i \in C \cap Z$ is:

$$s_{\text{out}}(e_i \in C \cap Z) = \frac{1}{|C \setminus Z|} \cdot \sum_{e_j \in C \setminus Z} w_{ij}$$

Likewise, for some non-SOZ electrode $e_i \in C \setminus Z$, the modified local out-strength is:

$$s_{\text{out}}(e_i \in C \setminus Z) = \frac{1}{|C \cap Z|} \cdot \sum_{e_j \in C \cap Z} w_{ij}$$

The modified local out-strength therefore reflects the extent to which an electrode which is an SOZ, or not an SOZ, electrode leads activity in other electrodes within the same community that are not, or are, SOZ electrodes, respectively. Modified in-strengths are computed similarly. The modified strength is defined only for electrodes within communities that were deemed significant after permutation test, and which have at least one SOZ electrode and at least one non-SOZ electrode.

We were also interested in the extent to which in- and out-strength differed from each other in a single electrode, and, therefore, the degree to which an electrode's tendency to lead or be led is asymmetric. We thus computed the relative difference between the absolute out-strength and in-strength for each electrode. This metric is defined as the relative out-strength, $r_{\text{out}}(e_i)$ for each elec-

trode e_i, which is the additive inverse of the relative in-strength $r_{out}(e_i)$:

$$r_{out}(e_i) = \frac{s_{out}(e_i) - s_{in}(e_i)}{s_{out}(e_i) + s_{in}(e_i)}$$

The relative out-strength may be computed using standard, local, or modified absolute out- and in-strengths.

2.6. IED sleep-wake asymmetry

Based on the mean IED rate during all awake and asleep epochs for each electrode, we defined the sleep-wake asymmetry as:

$$\frac{\bar{f}_{sleep} - \bar{f}_{awake}}{\bar{f}_{sleep} + \bar{f}_{awake}}$$

where $\bar{f}_{sleep}$ and $\bar{f}_{awake}$ are the mean IED rates across all asleep and awake epochs, respectively, for each electrode.

3. Results

We examined intracranial EEG (iEEG) recordings in nine participants (six female; mean age 39.9, range 20–58) who were being monitored for seizure activity using surgically placed intracranial subdural and depth electrodes. Implantations were performed for clinical reasons including lack of imaging findings, uncertainty about seizure focus lateralization, or dual pathology. Patient information, including demographic and clinical data, are provided in Table 1. In brief, seven of the nine patients included in our study had temporal lobe epilepsy and proceeded to temporal lobe resections. One patient had a parietal resection, and one patient with extra-temporal lobe epilepsy had no resection due to poorly localized seizure onsets (Figs. S1 and S2). Of the 8 patients with resections, post-operative seizure outcomes included 4 patients with Engel class 1, 2 with Engel class 2, and 1 with Engel class 3 outcomes; one patient was lost to follow up.

Each long-term monitoring session was divided into two-hour epochs by the recording system. We examined, on average, 6 ± 1 (mean $\pm$ SD; median 6, range 5–8) epochs in each participant for the presence of IEDs. These included 3.2 ± 0.83 asleep epochs (median 3, range 5–8) and 2.8 ± 0.44 awake epochs (median 3, range 2–3) in each participant, comprising 8.1 ± 3.6 and 6.7 ± 2 h, respectively. Based only on ictal iEEG recordings, and on previously established criteria (Marsh et al., 2010), an epileptologist blinded to our analysis determined which electrodes participated in seizure onset. We designated these electrodes as SOZ (seizure onset zone) electrodes. All other electrodes were designated as non-SOZ electrodes.

3.1. Automated community detection

We were interested in characterizing the relationships between electrode pairs based on the tendency of IED activity in one electrode to lead IED activity in the other. Such a relationship would suggest that the two electrodes exhibit a functional coupling.

We first used a custom-built automated IED detector to identify IED events in every electrode in every epoch extracted for analysis (Fig. 1; see Methods, Section 2.2, Automated IED detection). On average, we identified 81 ± 13 electrodes per participant that demonstrated IED activity. The average IED rate among these electrodes was 1.1 ± 1.2 IED per minute. This amounted to a mean total number of IED events of 927 ± 1018 per electrode, over all epochs considered. The IED rate in SOZ electrodes was 1.3 ± 0.98, compared to 1.1 ± 1.3 in non-SOZ electrodes. There was no significant difference in IED rates between these groups ($t(591) = 1.56, p = 0.12$).

We then established a bi-directional measure of coupling strength between electrodes, defined as the probability of observing an IED in one electrode, given that a IED occurred in another (see Methods, Section 2.3, IED coupling between electrodes). Based on these coupling strengths, we used an automated procedure to sort electrodes into communities that each exhibited strong coupling among its members (Fig. 2a–c; see Methods, Section 2.4, Automated community detection). Hence, in an unsupervised fashion, electrodes were assigned to groups such that, within each group, coupling strengths were significantly higher than would be expected by chance. The resultant communities in a single participant are shown in Fig. 2c-e. Across participants, we identified 33 communities containing a total of 583 electrodes. Mean pairwise distance between electrodes within each community was 4.49 ± 2.02 cm.

We designated each algorithmically identified community as either Type 1 or Type 2, depending on whether at least 10% of the electrodes in a given community were designated as SOZ electrodes (see Methods, Section 2.4, Automated community detection). In this manner, we designated 11 communities as Type 1. Each participant had median 4 (range $1-6$) communities, of which median 1 (range 0–3) were Type 1. Each Type 1 community contained a total of 20.00 ± 14.08 electrodes, of which on average 26.0 ± 25 percent were SOZ electrodes. Each Type 2 community contained a total of 16.95 ± 12.90 electrodes, of which on average 1.0 ± 2.0 percent were SOZ electrodes. Every participant had at least one community containing SOZ electrodes. However, since Type 1 communities required 10% or greater SOZ electrodes, two participants (IDs 2 and 7) had no Type 1 communities. Information about community count, SOZ content, and anatomic locations are provided in Table 2.

3.2. SOZ electrodes lead IED activity within Type 1 communities

Given that SOZ electrodes are designated as the electrodes in which seizures, and by extension pathologic interictal activity, are presumed to originate, we hypothesized that IED activity in the SOZ electrodes would lead IED activity in other electrodes within the Type 1 communities. We explored this hypothesis using each electrode's out- and in-strength, which reflect the extent to which an electrode exhibits IED activity that leads, or is led by, other electrodes. We found that, within Type 1 communities, the electrodes with the greatest out-strength tended to be the SOZ electrodes (Fig. 2d, f). In virtually all participants, the clinically-identified SOZ electrodes overlapped with the electrode or electrodes with maximal out-strength within their community (Figs. S1 and S2). Our findings suggest that those brain regions that ultimately give rise to seizures lead IED activity within cortical networks. These findings are consistent with previous work demonstrating that electrodes which lead sequences of IEDs tend to lie within the SOZ (Alarcon et al., 1997; Hufnagel et al., 2000). However, our findings build upon this previous work to illustrate the probabilistic basis by which electrodes depend on the SOZ to give rise to IEDs.

We sought to further explore the nature of the coupling relationships within Type 1 communities, including the relationship between SOZ and non-SOZ electrodes. We hypothesized that the tendency of SOZ electrodes to lead the global network (Fig. 2f) stemmed in particular from SOZ electrodes leading non-SOZ electrodes within Type 1 communities. We therefore examined the contribution of global and local out-strengths (see Methods, Section 2.5, Electrode leading and susceptibility) to the tendency of SOZ electrodes to lead other electrodes. Across all participants, the mean global out-strength was significantly higher among SOZ electrodes (0.0046 ± 0.0036), compared to non-SOZ electrodes (0.003 ± 0.0024; $t(725) = 5.20, p < .001$). In addition, across all

Table 2
Anatomic locations of communities and resections in study participants. A key is provided following the table. Colors in the **cluster type** column correspond to the colors used in Figs. 2, S1, and S2.

Patient	Total comm-unities	Number of total leads	Number of SOZ leads	Number resected leads	Comm-unity Type	Locations, SOZ	Locations, non-SOZ	Locations, resected
1	5	16	0	0			G, MST, PST, TO	
		17	3	5		MST, PST, TT	G, OF, PST, TT	G, MST, TT
		13	0	0			AST, LF, MST, OF, TP, TT	
		5	0	0			PPST, TP	
		4	0	0			G	
2	1	29	1	2		TT	AST, G, LF, OF, P, PST, TT	AST, TT
3	4	12	10	11		G, RAST, RPST, RTT	RMST, ROF	G, RAST, RMST, RPST, RTT
		5	0	5			G	G
		13	0	5			G, LPLT	G
		49	0	3			G, LALT, LAST, LPLT, LPST, RIF, ROF, RP, RPST, RSF, RTT	G, RPST, RTT
4	5	32	3	1		G	G, LF, MO, MST, OF, PP, SO	G
		19	3	0		MO, PST	G, IO, LP, PP, PPST, SO	
		13	3	6		AST, TT	AST, G, LF, LP, PP, TT	AST, G, TT
		9	6	0		G, PPST, PST	IO	
		7	0	0			G, TT	
5	3	36	1	6		G	G, LAST, LF, LMST, OF, P, RALT, RAST, RPLT, TT	G, LAST, LMST, TT
		16	0	0			G, LPST, P, PPST, RPLT, RPST	
		10	1	7		TT	G, LMST, TT	G, LMST, TT
6	2	44	9	14		AST, MST, PST, TT	G, LF, LP, MST, OF, TT	AST, G, MST, TT
		9	1	3		G	G	G
7	3	15	0	1			G, IF, ILT, MLT, PLT, PST, SF, SLT	PST
		41	2	16		ATT	AST, ATT, G, IF, MLT, PLT, PST, SF, SLT	AST, ATT, PLT, PST, SLT
		16	0	0			G, ILT	
8	6	10	0	1			RAST, RAT, RPP, RPST	RPP
		46	7	6		RMF, RPF, RSM	LPT, RAF, RAP, RAT, RMF, RMP, ROP, RPF, RPIH, RPP, RPST, RPT, RSM	RMP, ROP, RPP
		9	1	1		RPP	LAST, LAT, LPST, RAT	RPP
		3	0	0			LAST, LPST	
		23	1	2		RMF	RAP, RAST, RAT, RMP, ROP, RPIH, RPP, RPST, RPT	RAP, ROP
		4	0	0			LAST, LAT, LPST	
9	4	32	5	0		AIP, IP	AIF, AIP, ASF, ASP, AST, IP, LF, PF, PIP, PSP	
		8	0	0			AIP, IP, PIP, PSP	
		11	0	0			AIP, ASP, IP, LF, PF, PIP, PSP	
		17	0	0			AIF, ALT, ASF, AST, LF, PST	

Key: Shades of red: Type 1 community. Shades of blue: Type 2 community.
The colors used in the community type column map onto the colors used in Figs. 2, S1, and S2.
L: Left. R: right. AF: anterior frontal. AIF: anterior inferior frontal. AIP: anterior inferior parietal. ALT: anterior lateral temporal. AP: anterior parietal. ASF: anterior superior frontal. ASP: anterior superior parietal. AST: anterior subtemporal. AT: anterior temporal. ATT: anterior temporal tip. F: lateral frontal. G: temporal grid. IF: inferior frontal. ILT: inferior lateral temporal. IO: inferior occipital. IP: inferior parietal. MF: middle frontal. MLT: middle lateral temporal. MO: left middle occipital. MP: middle parietal. MST: middle subtemporal. OF: orbitofrontal. OP: occipito-parietal. P: parietal. PF: posterior frontal. PIH: posterior interhemispheric. PIP: posterior inferior parietal. PLT: posterior lateral temporal. PP: posterior parietal. PPST: posterior posterior subtemporal. PSP: posterior superior parietal. PST: posterior subtemporal. PT: posterior temporal. SF: superior frontal. SLT: superior lateral temporal. SM: sensorimotor. SO: superior occipital. TO: temporo-occipital. TP: temporo-parietal. TT: temporal tip.

participants, the mean local out-strength was also significantly higher among SOZ electrodes (0.014 ± 0.017) compared to non-SOZ electrodes ($0.0087 \pm 0.012; t(591) = 3.09, p < 0.001$). Thus, SOZ electrodes tended to lead IEDs in both global and local networks.

We also examined whether SOZ electrodes tended to lead IEDs more strongly than non-SOZ electrodes if we only considered coupling from electrodes within communities to those outside them. We therefore computed the external out-strength for each electrode, which specifically quantifies the extent to which each electrode leads electrodes that lie outside of its community (see Methods, Section 2.5, Electrode leading and susceptibility). We found no difference between external out-strength in SOZ electrodes (0.0019 ± 0.002) compared to non-SOZ electrodes ($0.0016 \pm 0.0015; t(591) = 1.00, p = 0.32$). As expected by virtue of the design of our community detection algorithm, the local out-strength was much greater than the external out-strength in SOZ electrodes ($t(112) = 5.43, p < 0.001$), as well as in non-SOZ electrodes ($t(1070) = 13.97, p < 0.001$). Thus, the tendency of SOZ electrodes to lead the global network stems primarily from their activity within local communities.

To explicitly investigate the coupling relationship between SOZ and non-SOZ electrodes, we computed the modified out-strength,

which excludes all relationships within each SOZ or non-SOZ category and focuses only on relationships across categories (Fig. 3a, b, see Methods, Section 2.5, Electrode leading and susceptibility). We only analyzed these relationships in Type 1 communities, since these are the communities in which SOZ electrodes were likely to be present and exert influence. SOZ electrodes had significantly greater modified out-strength compared to non-SOZ electrodes (0.016 ± 0.025 versus $0.0046 \pm 0.0083, t(218) = 5.25, p < .001$; Fig. 3c, d). SOZ electrodes also had significantly greater relative out-strength compared to non-SOZ electrodes (0.21 ± 0.40 versus $-0.17 \pm 0.55, t(218) = 4.49, p < .001$; Fig. 3c, e; see Methods, Section 2.5, Electrode leading and susceptibility). There was no significant difference in in-strength between electrode groups, although SOZ electrodes had slightly greater in-strength than non-SOZ electrodes (0.0097 ± 0.016 in SOZ electrodes versus 0.007 ± 0.0057 in non-SOZ electrodes; $t(218) = 1.11, p = 0.27$). Together, these data support the hypothesis that within Type 1 communities, IED activity in SOZ electrodes leads IED activity in non-SOZ electrodes.

3.3. State variability of IED activity

Given that the identified communities indeed reflect functional coupling between brain regions, IED activity between coupled brain regions might covary dynamically with physiological state. To explore this, we examined how the transmission of IED activity from the SOZ to susceptible surrounding brain regions differs in awake versus asleep states. Previous evidence has suggested that physiologic states such as sleep may modulate IED rates (Sammaritano et al., 1991; Malow et al., 1999; Varotto et al., 2012; Clemens et al., 2005; Francione et al., 2003; Lambert et al., 2018), and so we hypothesized that state-related variability in IED activity within epileptogenic regions may influence state-related variability in surrounding brain tissue through the functional coupling that we have identified thus far.

The overall mean IED rate was greater in the awake state compared to the asleep state (1.2 ± 1.9 versus $0.97 \pm 0.9; t(726) = 4.62, p < 0.001$). However, the overall rate of IEDs across all electrodes does not account for any differences that may arise within each type of electrode. We thus evaluated IED rate during awake and asleep states, considering community and electrode types separately.

Consistent with previous findings (Sammaritano et al., 1991; Malow et al., 1999; Varotto et al., 2012; Clemens et al., 2005; Francione et al., 2003; Lambert et al., 2018), SOZ electrodes demonstrated 1.7 ± 1.4 IEDs per minute during sleep compared to 0.91 ± 0.71 per minute during awake states. For non-SOZ electrodes, however, asleep and awake IED rates were 0.89 ± 0.85 and 1.3 ± 2.2, respectively. Of note, non-SOZ electrodes are present in substantial numbers in both Type 1 and Type 2 communities. In non-SOZ electrodes within Type 1 communities, the mean IED rate during asleep and awake epochs was 0.88 ± 0.76 versus 1.1 ± 2.8 respectively. Meanwhile, non-SOZ electrodes in Type 2 communities exhibited a mean IED rate during asleep and awake epochs of 0.89 ± 0.88 versus 1.4 ± 1.8, respectively.

To explore this further, we established a metric for state variability, the sleep-wake asymmetry, that captures the extent to which IED rates vary between the sleep and awake states while controlling for the absolute value of these rates (see Methods, Section 2.6, IED sleep-awake asymmetry). This metric ranges between 1 and −1, depending on whether IEDs are only observed during sleep or during the awake state, respectively, and takes a value of 0 if the IED rate is unchanged between the two states. The sleep-wake asymmetry was significantly greater than zero in Type 1 community electrodes ($t(219) = 4.41, p < 0.001$, one-sample t-test) and significantly less than zero in Type 2 community electrodes ($t(372) = 6.75, p < 0.001$, one-sample t-test. The sleep-wake asymmetries of electrodes within Type 1 and Type 2 communities were also significantly different from one another (0.12 ± 0.4 versus $-0.12 \pm 0.33; t(591) = 7.7, p < 0.001$; Fig. 4a).

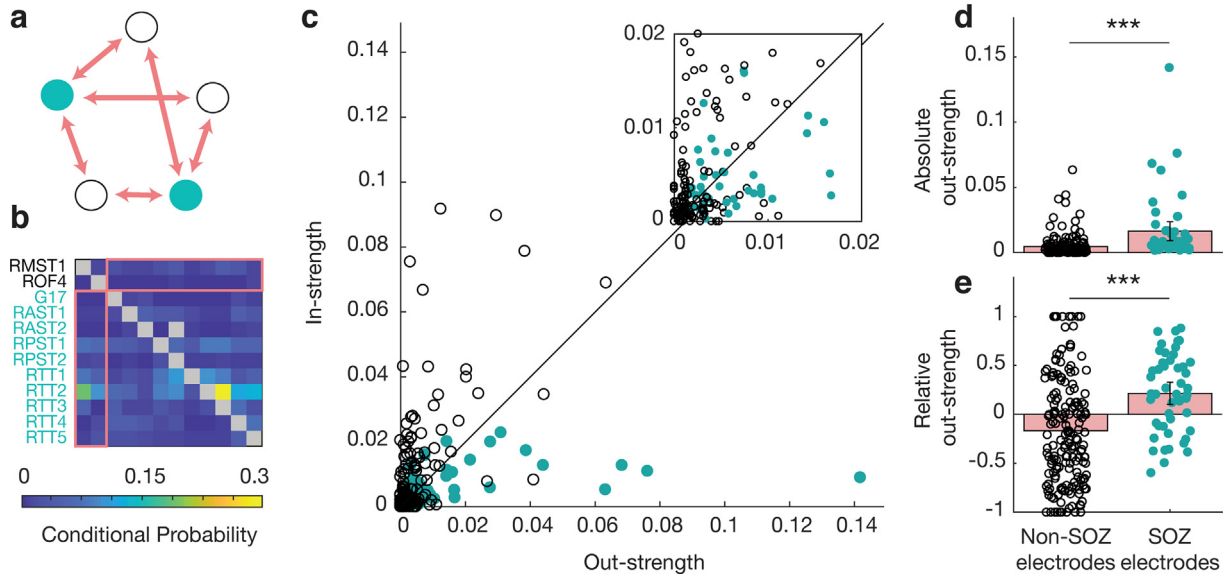

Fig. 3. Relationship between SOZ and non-SOZ electrodes in Type 1 clusters. **(a)** We were interested in considering the influence of SOZ electrodes on non-SOZ electrodes, and vice versa. Therefore, we developed the *modified* out-strength, which considers only the relationships between electrode types, and not within electrode types (see Section 2.5, Electrode leading and susceptibility). This approach is schematized in **a**. **(b)** provides an additional schematic illustration of the modified out- and in-strengths. We only considered cells of the community adjacency matrix which correspond to the coupling strengths between electrodes of differing SOZ status. RTT: right temporal tip; RAST: right anterior subtemporal; RPST: right posterior subtemporal; ROF: right orbitofrontal; RAST: right anterior subtemporal; G: grid. **(c)** Here, the modified in-strength is plotted against the modified out-strength for all Type 1 community electrodes. We can see that SOZ electrodes tend to have a greater absolute out-strength than non-SOZ electrodes. SOZ electrodes also tend to lie below the diagonal, corresponding to a positive relative out-strength, while non-SOZ electrodes tend to lie above the diagonal. **(d)** Comparison of out-strength in SOZ versus non-SOZ electrodes. The SOZ electrodes have a significantly greater absolute modified out-strength ($p < 0.001$). Error bars indicate 95% confidence interval. **(e)** Comparison of relative out-strength in SOZ versus non-SOZ electrodes. The SOZ electrodes have a significantly greater relative modified out-strength ($p < 0.001$). Error bars indicate 95% confidence interval. The results shown in **c-e** suggest that, within Type 1 clusters, SOZ electrodes drive IED activity in non-SOZ electrodes.

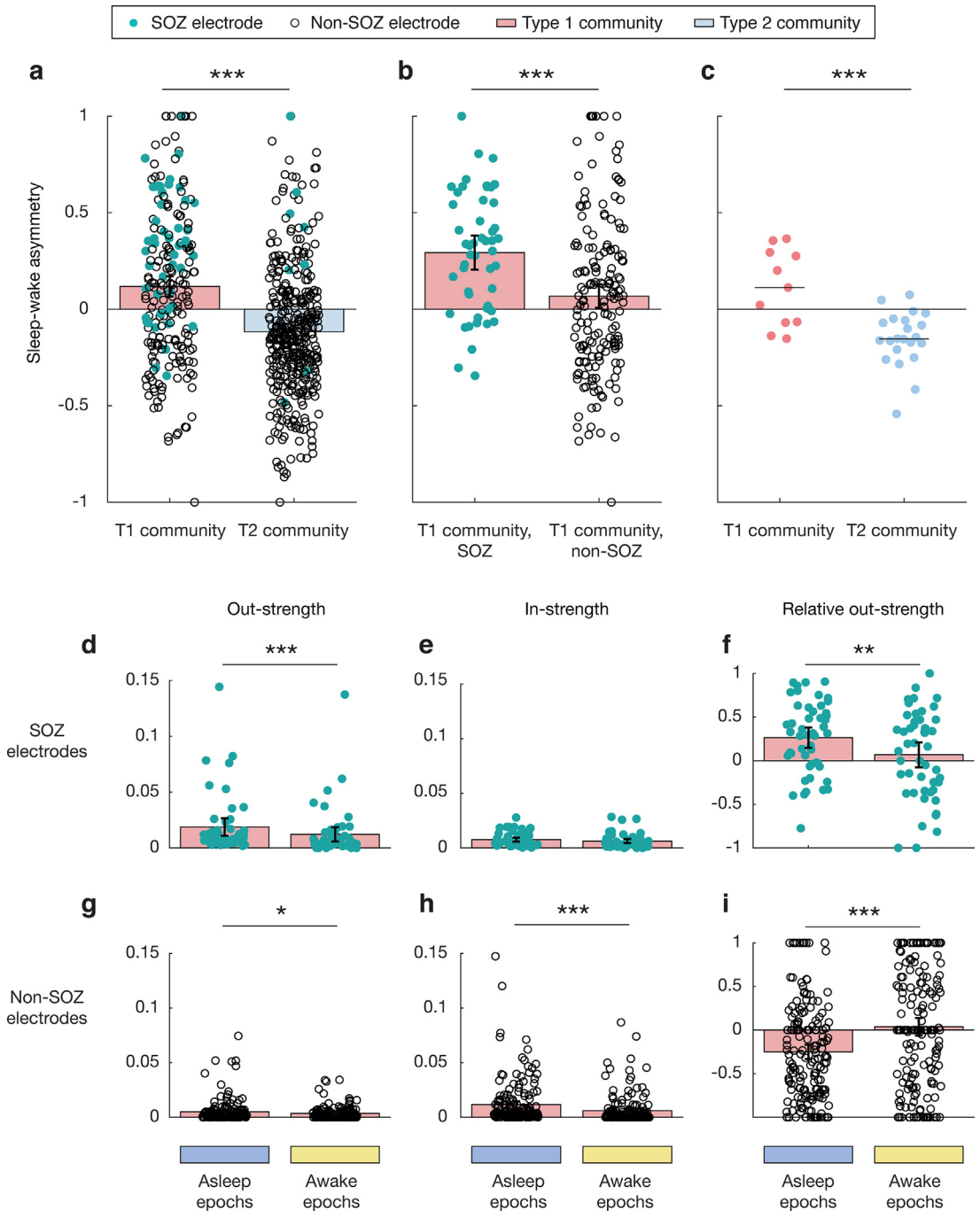

Fig. 4. The effect of physiologic state on coupling strength and IED activity. **(a)** Sleep-wake asymmetry reflects the extent to which IED activity is different between the sleep and awake states (see Methods, Section 2.6, IED sleep-wake asymmetry). In Type 1 communities, the sleep-wake asymmetry is significantly positive ($p < 0.001$), corresponding to a greater IED rate in the asleep state. On the other hand, the sleep-wake asymmetry is significantly negative in Type 2 communities ($p < 0.001$), indicating that IED rates are greater in the awake state. The sleep-wake asymmetry is significantly different between the two groups ($p < 0.001$). **(b)** Sleep-wake asymmetry in SOZ versus non-SOZ electrode within Type 1 communities. Notably, the sleep-wake asymmetry is significantly positive in both groups ($p < 0.001$ in SOZ electrodes; $p < 0.05$ in non-SOZ electrodes. The sleep-wake asymmetry is also significantly different between the two groups ($p < 0.001$). **(c)** Sleep-wake asymmetry is computed at the level of the community; each dot represents a community mean. There is a significant difference between Type 1 and Type 2 community means ($p < 0.001$), consistent with the findings in **a**. Moreover, there is a substantial effect size between the two groups; Cohen's $d = 1.51$. When used to distinguish between Type 1 and Type 2 clusters, the sleep-wake asymmetry yields an area under the receiver operating characteristic curve of 0.86. The robust difference in sleep-wake asymmetry at the cluster level likely stems from the covariance in IED activity within cluster members (panels **a** and **b**). **(d)** The absolute modified out-strength is provided for SOZ electrodes in asleep and awake states (see Section 2.5, Electrode leading and susceptibility). Out-strength in SOZ electrodes is significantly-greater in the asleep state than in the awake state ($p < 0.001$). **(e)** The absolute modified in-strength in SOZ electrodes in asleep and awake states. There is no significant difference between in-strength in asleep versus awake states. **(f)** The relative modified out-strength in SOZ electrodes in asleep and awake states. The relative out-strength is significantly greater in the asleep state ($p < 0.001$). **(g)** The absolute modified out-strength in non-SOZ electrodes in asleep and awake states. There is a modest, but statistically significant, increase in out-strength in the asleep state compared to the awake state ($p < 0.05$). **(h)** The absolute modified in-strength for non-SOZ electrodes. There is a significant increase in in-strength among these electrodes in the asleep state ($p < 0.001$). Along with the results in panel **d**, these results suggest that sleep promotes the coupling between SOZ and non-SOZ electrodes, and that, in the setting of this coupling, SOZ electrodes act as the driver of IED activity. **i)** The relative modified out-strength for non-SOZ electrodes. The opposite effect to that in **f** is seen, in that the relative out-strength is less (and thus the relative in-strength is greater) in the asleep state compared to the awake state ($p < 0.001$). Error bars indicate 95% confidence interval.

Next, we considered sleep-wake asymmetry in Type 1 communities, separated by electrode type. In Type 1 community SOZ electrodes, sleep-wake asymmetry was significantly greater than zero ($t(48) = 6.64, p < 0.001$, one-sample t-test). Notably, sleep-wake asymmetry was also significantly greater than zero in Type 1 community non-SOZ electrodes ($t(170) = 2.19, p < 0.05$, one-sample t-test). The positive sleep-wake asymmetry in these non-SOZ electrodes is in sharp contrast with the negative sleep-wake asymmetry seen in Type 2 electrodes, which are also virtually all non-SOZ. The sleep-wake asymmetries in Type 1 community SOZ and non-SOZ electrodes were also significantly different from each other (0.29 ± 0.31 versus 0.068 ± 0.41; $t(218) = 3.59, p < 0.001$; Fig. 4b).

The similar state-related behavior observed in both SOZ and non-SOZ electrodes within Type 1 communities suggests that IED activity in these brain regions may arise from a similar underlying pathophysiology. We therefore examined sleep-wake asymmetry at the level of Type 1 and Type 2 communities and found a significant difference between sleep-wake asymmetry at the community level (Cohen's $d = 1.51$; 0.11 ± 0.2 in Type 1 communities versus -0.15 ± 0.14 in Type 2 communities; $t(31) = 4.35, p < 0.001$; Fig. 4c). We constructed a receiver operating characteristic (ROC) curve with variable thresholds and found that the sleep-wake asymmetry could accurately distinguish Type 1 from Type 2 clusters (AUC 0.86, 95% CI 0.76–0.95), suggesting that IED behavior and modulation by sleep tend to be more uniform at the level of the community than at the level of the individual electrode.

To examine whether the coupling between SOZ and non-SOZ electrodes is modulated by sleep compared to the awake state, we then separately analyzed in-strengths and out-strengths for SOZ and non-SOZ electrodes during either asleep or awake epochs. SOZ electrodes had a greater out-strength in the asleep state than in the awake state (0.019 ± 0.027 versus 0.012 ± 0.023; $t(48) = 3.76, p < 0.001$, paired t-test), but no difference in in-strength (0.0076 ± 0.0065 asleep versus 0.0063 ± 0.0066 awake; $t(48) = 1.49, p = 0.14$, paired t-test; Fig. 4d, e). This resulted in a significant sleep-wake difference in the relative out-strength of SOZ electrodes (0.26 ± 0.41 asleep versus 0.067 ± 0.5 awake; $t(48) = 3.47, p < 0.01$, paired t-test; Fig. 4f). On the other hand, non-SOZ electrodes exhibited both a greater out-strength during sleep compared to the awake state (0.005 ± 0.011 asleep versus 0.0035 ± 0.0057 awake; $t(170) = 2.47, p < 0.05$, paired t-test) and a greater in-strength (0.012 ± 0.02 versus 0.0061 ± 0.013; $t(170) = 3.96, p < 0.001$, paired t-test; Fig. 4g, h). This also resulted in a significant sleep-wake difference in the relative out-strength of non-SOZ electrodes (-0.25 ± 0.55 asleep versus 0.037 ± 0.67 awake; $t(170) = 4.76, p < 0.001$, paired t-test; Fig. 4i). These results suggest that transmission of pathological activity from SOZ to non-SOZ electrodes over local epilepsy networks is heightened in the asleep state.

Given the observed differences in strength between SOZ and non-SOZ electrodes, and the observed modulation of IED activity by physiologic state, we sought to use these features to determine whether or not a given electrode lies within the SOZ. We therefore used multiple linear regression to classify electrodes as SOZ or non-SOZ, using in-strength, out-strength, relative out-strength, and sleep-wake asymmetry as input parameters. For the purposes of classification,we used all 727 electrodes, and not just the 583 retained after permutation testing, since permutation testing may unfairly retain those members of the electrode population which are easy to classify. There was a significant effect between these parameters and SOZ identity ($F(5, 721) = 18.1, p < 0.001, R^2 = 0.11$). Examining the individual predictors revealed that in-strength ($t = 2.94, p < 0.01$), relative out-strength ($t = 3.02, p < 0.01$), and sleep-wake asymmetry ($t = 7.24, p < 0.001$) were significant predictors in the model. Area under the receiver operating characteristic curve generated by the linear model's prediction was 0.78, suggesting that classification at the level of individual electrodes is successful, although slightly more difficult than distinguishing Type 1 and Type 2 communities.

3.4. Outcome after resection

We were interested in exploring the relationship between surgical resection of the identified communities and post-surgical outcome. Of the nine participants, only seven had a surgical resection and sufficient follow-up to examine this question. We found that patients obtaining seizure freedom (Engel class 1) had a significantly greater percentage of electrodes resected compared to those that had poorer seizure outcomes ($31.5 \pm 10.5\%$ versus $10.0 \pm 1.0\%$; $t(5) = 3.43, p < 0.05$). This is consistent with previous research, which has linked increased extent of resection with improved outcome (Awad et al., 1989; Nayel et al., 1991). However, our findings may simply reflect an increased density of electrodes overlying the area which was ultimately resected.

We hypothesized that the Type 1 community was the locus of initiation and spread of pathological activity, and therefore that resection of Type 1 community leads, in particular, may yield good outcome. We found a greater proportion of Type 1 leads were resected in participants who obtained seizure freedom compared to those that did not ($64.7 \pm 30.4\%$ versus $21.0 \pm 11.3\%$), but these differences were not statistically significant ($t(3) = 1.86, p = .16$). This is likely related to the fact that, with only seven participants who received resection, our data are underpowered to fully examine this effect. There was no significant difference in the proportion of SOZ electrodes resected in participants obtaining seizure freedom compared to those that did not ($70.5 \pm 47.8\%$ versus $59.09 \pm 44.9\%$; $t(5) = .32, p = .76$), suggesting that if there were any benefits that may arise from resecting Type 1 community electrodes, they were not simply due to increased resection of SOZ electrodes alone.

4. Discussion

Here we describe a novel, probabilistic approach for identifying communities of functionally-coupled IED events within the irritative zone in patients with focal epilepsy. Within these communities, we explore the extent to which brain regions exhibiting IED activity lead or are led by IEDs in other functionally-coupled areas. We found that, in general, the SOZ showed a greater tendency to lead IED activity than other brain regions to which it is coupled, consistent with previous descriptions of propagation of abnormal activity from the SOZ into relatively less pathologic surrounding regions. We next examined how entrainment relationships within communities change with physiologic state. We found increased susceptibility to involvement in pathologic activity during sleep in areas functionally coupled to the SOZ. This dynamic coupling may help to explain the increased field of IEDs that has often been observed during sleep.

For the purposes of presurgical planning, there is significant interest in using interictal recordings to predict the brain regions that will go on to generate seizures, since IEDs tend to be frequent while clinical seizures may be quite rare. While by definition the SOZ is involved in the initiation and subsequent propagation of seizures, it is generally hypothesized to play a critical role in the generation of interictal activity as well. Although the irritative zone usually overlaps with the SOZ, it is often much larger (Bartolomei et al., 2016), creating the desire to stratify the relative degree of epileptogenicity within the irritative zone, in order to identify those regions most likely to be involved in the generation of clinical seizures (Bartolomei et al., 2016; Luders et al., 2006).

This has not been straightforward, as studies attempting to identify the SOZ using single electrode attributes such as highest IED rates or highest amplitudes have met with only modest success (Asano et al., 2003; Hufnagel et al., 2000; Marsh et al., 2010; Goncharova et al., 2013; Bartolomei et al., 2016). Additionally, although resection of tissue demonstrating frequent IEDs in addition to the SOZ correlates with improved post-operative seizure control in some studies (Paolicchi et al., 2000; Krsek et al., 2009), other studies suggest that the removal of all areas generating IEDs is often not required to achieve seizure freedom postoperatively (Wyllie et al., 1987).

An alternate approach toward understanding the relationship between the irritative and seizure onset zones is to consider the interactions within these brain regions. Using our algorithmic community detection procedure, we found that the irritative zone was in fact heterogeneous and dynamic. As previously described and as often seen clinically, we found that in a given patient the irritative zone may be composed of independent subnetworks or communities, which may be located in different lobes or even hemispheres (Hufnagel et al., 2000). In addition, we found variable conditional probabilities of IED co-occurrence between electrode pairs within each community, consistent with the well-described variability between individual IEDs due to differences in propagation and field spread (de Curtis and Avanzini, 2001; Sabolek et al., 2012; Janca et al., 2018; Alarcon et al., 1994).

Although activity within an IED community is variable, the SOZ is still presumed to play a critical role in generating IEDs (de Curtis and Avanzini, 2001). Previous studies have found consistently elevated functional or effective connectivity within epileptogenic regions using a variety of measures, even in the interictal state (Varotto et al., 2012; Wilke et al., 2010; Korzeniewska et al., 2014; Lambert et al., 2018). Graph theoretic approaches have similarly found that epileptogenic regions tend to serve as hubs, playing an important role in interictal activity as well as seizure onset and propagation (Morgan and Soltesz, 2008; Wilke et al., 2011; Varotto et al., 2012; Korzeniewska et al., 2014; Chiang and Haneef, 2014).

We sought to further describe the role of the SOZ in the initiation and propagation of interictal activity within our communities by examining the conditional probabilities of IED activity across electrodes. By definition, the electrodes we identified as having the largest absolute out-strength tended to lead IED activity in the remaining electrodes within the community. In our data, the SOZ electrodes had greater absolute and relative out-strength than non-SOZ electrodes. Previous studies of propagation patterns within IED communities have similarly shown that leading electrodes tended to be localized within the SOZ (Hufnagel et al., 2000; Asano et al., 2003; Alarcon et al., 1997). Variability in propagation patterns, particularly in the identity of the leading electrode within an IED community, have limited these approaches, while probabilistic methods such as ours explicitly take this variability into account. Other studies using similar approaches have also found that outflow measures appear to be more sensitive than inflow measures for identifying the SOZ (Varotto et al., 2012; Wilke et al., 2011; Jung et al., 2011), and nodes with the highest values of out-degree and betweenness centrality tend to be located within epileptogenic lesions or the SOZ (Varotto et al., 2012; Wilke et al., 2011; Van Mierlo et al., 2011).

As state variability is characteristic of IEDs, we used our probabilistic framework to investigate the state-dependent dynamics of the coupling within our communities. Numerous studies have described modulation of IED activity by state of arousal, with increased frequency and spatial extent of IEDs during NREM sleep (Sammaritano et al., 1991; Steriade et al., 1994; Malow et al., 1999; Varotto et al., 2012; Janca et al., 2018; Clemens et al., 2005; Lambert et al., 2018), possibly due to the increased temporal and spatial synchronization that occurs during this state (Staba et al., 2002; Le Van et al., 2016; Clemens et al., 2005; Francione et al., 2003; Lambert et al., 2018). We found increased IED rates during sleep in the SOZ, and a similar sleep-wake asymmetry in the non-SOZ areas that are functionally coupled to the SOZ. The opposite sleep-wake asymmetry was seen in Type 2 community electrodes, which may partly explain the mixed results previously reported in the literature regarding IED state variability. Indeed, the difference in behavior between non-SOZ electrodes in Type 1 communities and non-SOZ electrodes in Type 2 communities may be due to the fact that non-SOZ electrodes in Type 1 communities are functionally-coupled to the SOZ; the SOZ electrodes in these communities may be the primary drivers of increased IED activity in the asleep state. This hypothesis maps very closely onto previous work, which found a gradated effect of sleep on IED rate given the relationship to the SOZ (greatest sleep-wake difference in SOZ; intermediate in propagation zone; and least in non-involved regions (Lambert et al., 2018)).

Evaluation of the sleep-wake asymmetry of IED rates at the community level revealed a substantial difference between Type 1 and Type 2 communities, in fact allowing for robust classification of community type. We found an increase in out-strength in SOZ electrodes during sleep, as well as an increase in the in-strength in non-SOZ electrodes in Type 1 communities. These findings provide evidence that sleep drives the initiation and propagation of pathologic activity in neighboring brain regions, and are consistent with the increased field spread of IED activity during sleep that has been reported previously (Sammaritano et al., 1991; Malow et al., 1999; Emerson et al., 1995). Seizures and IEDs may be co-modulated by similar factors operating at multiple time scales, including the sleep-wake cycle, as well as metabolic, genetic, hormonal, environmental, and brain circuit influences (Karoly et al., 2016; Baud et al., 2018; Jirsa et al., 2014; Lambert et al., 2018). Variability in IED rates may therefore be useful as a biomarker of disease activity or seizure susceptibility.

The gold standard for establishment of the location of the epileptogenic zone, as opposed to the observed seizure onset zone, remains seizure freedom following surgery (Luders et al., 2006). Although not significant in this small group of patients, we did note a trend toward improved seizure outcome with the resection of brain regions encompassing Type 1 communities. However, in order to establish the clinical applicability of our findings with respect to identification of the epileptogenic zone, further study is required. This should involve a larger patient cohort, including seizure free and not seizure free patients.

In this work, we describe an automated probabilistic algorithm for detecting communities of interictal epileptiform activity, as well as a graph-theoretical approach to investigating the dynamics within these communities. Together, our data provide evidence for the presence of small networks within the irritative zone, with core foci that propagate epileptiform activity to less pathological but nonetheless coupled brain regions. In the networks that go on to generate seizures, this propagation into surrounding tissue appears to be facilitated by sleep, consistent with other work describing increased rate and field extension of IEDs during sleep. State related variability in IED rates among these communities provided a robust metric for distinguishing communities containing the SOZ from those that did not. Automated detection of IED communities, as well as evaluation of state-dependent functional coupling and entrainment of pathological activity with these communities, may represent a powerful tool for the improvement of our understanding of the spatial and temporal variability that are hallmarks of both interictal and ictal activity in epilepsy.

Data for reference

Data and procedure for accurate soil sampling as mentioned in this study can be found at https://neuroscience.nih.gov/ninds/zaghloul/downloads.html.

Declaration of Competing Interest

None of the authors disclose any actual or apparent conflicts of interest which may have influenced the production of this manuscript.

Acknowledgements

This work was supported by the intramural research program of the National Institute for Neurological Disorders and Stroke. This research was also made possible through the NIH Medical Research Scholars Program, a public-private partnership supported jointly by the NIH and generous contributions to the Foundation for the NIH from the Doris Duke Charitable Foundation, the American Association for Dental Research, the Colgate-Palmolive Company, Genentech, Elsevier, and other private donors. Benjamin Diamond provided intellectual guidance. We are indebted to all patients who have selflessly volunteered their time to participate in this study.

Appendix A. Supplementary material

Supplementary data associated with this article can be found, in the online version, at https://doi.org/10.1016/j.clinph.2019.05.032.

References

Alarcon G, Garcia Seoane J, Binnie C, Martin Miguel M, Juler J, Polkey C, et al. Origin and propagation of interictal discharges in the acute electrocorticogram. implications for pathophysiology and surgical treatment of temporal lobe epilepsy. Brain: J Neurol 1997;120(12):2259–82.

Alarcon G, Guy C, Binnie C, Walker S, Elwes R, Polkey C. Intracerebral propagation of interictal activity in partial epilepsy: implications for source localisation. J Neurol Neurosurg Psychiatr 1994;57(4):435–49.

Asano E, Muzik O, Shah A, Juhasz C, Chugani DC, Sood S, et al. Quantitative interictal subdural eeg analyses in children with neocortical epilepsy. Epilepsia 2003;44(3):425–34.

Awad IA, Katz A, Hahn JF, Katz AKK, Ahl J, Lüders H. Extent of resection in temporal lobectomy for epilepsy. i. Interobserver analysis and correlation with seizure outcome. Epilepsia 1989;30(6):756–62.

Barrat A, Barthelemy M, Vespignani A. The architecture of complex weighted networks. Proc Natl Acad Sci 2007;101(11):3747–52.

Bartolomei F, Trébuchon A, Bonini F, Lambert I, Gavaret M, Woodman M, et al. What is the concordance between the seizure onset zone and the irritative zone? A seeg quantified study. Clin Neurophysiol 2016;127(2):1157–62.

Baud MO, Kleen JK, Mirro EA, Andrechak JC, King-Stephens D, Chang EF, et al. Multi-day rhythms modulate seizure risk in epilepsy. Nat Commun 2018;9(1):88.

Bourien J, Bartolomei F, Bellanger J, Gavaret M, Chauvel P, Wendling F. A method to identify reproducible subsets of co-activated structures during interictal spikes. application to intracerebral eeg in temporal lobe epilepsy. Clin Neurophysiol 2005;116(2):443–55.

Brown MW, Porter BE, Dlugos DJ, Keating J, Gardner AB, Storm PB, et al. Comparison of novel computer detectors and human performance for spike detection in intracranial eeg. Clin Neurophysiol 2007;118(8):1744–52.

Chapeton JI, Inati SK, Zaghloul KA. Stable functional networks exhibit consistent timing in the human brain. Brain 2017;140(3):628–40.

Chiang S, Haneef Z. Graph theory findings in the pathophysiology of temporal lobe epilepsy. Clin Neurophysiol 2014;125(7):1295–305.

Clemens Z, Janszky J, Clemens B, Szűcs A, Halász P. Factors affecting spiking related to sleep and wake states in temporal lobe epilepsy (tle). Seizure 2005;14(1):52–7.

de Curtis M, Avanzini G. Interictal spikes in focal epileptogenesis. Prog Neurobiol 2001;63(5):541–67.

Emerson RG, Turner CA, Pedley TA, Walczak TS, Forgione M. Propagation patterns of temporal spikes. Electroencephalogr Clin Neurophysiol 1995;94(5):338–48.

Expert P, Evans TS, Blondel VD, Lambiotte R. Uncovering space-independent communities in spatial networks. Proc Natl Acad Sci 2011;108(19):7663–8.

Francione S, Vigliano P, Tassi L, Cardinale F, Mai R, Russo GL, et al. Surgery for drug resistant partial epilepsy in children with focal cortical dysplasia: anatomical–clinical correlations and neurophysiological data in 10 patients. J Neurol Neurosurg Psychiatr 2003;74(11):1493–501.

Gaspard N, Alkawadri R, Farooque P, Goncharova II, Zaveri HP. Automatic detection of prominent interictal spikes in intracranial eeg: validation of an algorithm and relationsip to the seizure onset zone. Clin Neurophysiol 2014;125(6):1095–103.

Goncharova II, Spencer SS, Duckrow RB, Hirsch LJ, Spencer DD, Zaveri HP. Intracranially recorded interictal spikes: relation to seizure onset area and effect of medication and time of day. Clin Neurophysiol 2013;124(11):2119–28.

Gotman J, Marciani M. Electroencephalographic spiking activity, drug levels, and seizure occurence in epileptic patients. Ann Neurol 1985;17(6):597–603.

Hufnagel A, Dumpelmann M, Zentner J, Schijns O, Elger CE. Clinical relevance of quantified intracranial interictal spike activity in presurgical evaluation of epilepsy. Epilepsia 2000;41(4):467–78.

Janca R, Krsek P, Jezdik P, Cmejla R, Tomasek M, Komarek V, et al. The sub-regional functional organization of neocortical irritative epileptic networks in pediatric epilepsy. Front Neurol 2018;9:184.

Jirsa VK, Stacey WC, Quilichini PP, Ivanov AI, Bernard C. On the nature of seizure dynamics. Brain 2014;137(8):2210–30.

Jung YJ, Kang HC, Choi KO, Lee JS, Kim DS, Cho JH, et al. Localization of ictal onset zones in lennox-gastaut syndrome using directional connectivity analysis of intracranial electroencephalogr. Seizure 2011;20(6):449–57.

Karoly PJ, Freestone DR, Boston R, Grayden DB, Himes D, Leyde K, et al. Interictal spikes and epileptic seizures: their relationship and underlying rhythmicity. Brain 2016;139(4):1066–78.

Korzeniewska A, Cervenka MC, Jouny CC, Perilla JR, Harezlak J, Bergey GK, et al. Ictal propagation of high frequency activity is recapitulated in interictal recordings: effective connectivity of epileptogenic networks recorded with intracranial eeg. NeuroImage 2014;101:96–113.

Krsek P, Maton B, Jayakar P, Dean P, Korman B, Rey G, et al. Incomplete resection of focal cortical dysplasia is the main predictor of poor postsurgical outcome. Neurology 2009;72(3):217–23.

Lambert I, Roehri N, Giusiano B, Carron R, Wendling F, Benar C, et al. Brain regions and epileptogenicity influence epileptic interictal spike production and propagation during nrem sleep in comparison with wakefulness. Epilepsia 2018;59(1):235–43.

Le Van Quyen M, Muller LE, Telenczuk B, Halgren E, Cash S, Hatsopoulos NG, et al. High-frequency oscillations in human and monkey neocortex during the wake–sleep cycle. Proc Natl Acad Sci 2016;113(33):9363–8.

Leicht EA, Newman ME. Community structure in directed networks. Phys Rev Lett 2008;100(11):118703.

Lopes MA, Richardson MP, Abela E, Rummel C, Schindler K, Goodfellow M, et al. An optimal strategy for epilepsy surgery: disruption of the rich-club? PLoS Comput Biol 2017;13(8):e1005637.

Luders HO, Najm I, Nair D, Widdess-Walsh P, Bingman W. The epileptogenic zone: general principles. Epileptic Disord 2006;8(Suppl. 2):S1–9.

Malow BA, Selwa LM, Ross D, Aldrich MS. Lateralizing value of interictal spikes on overnight sleep-eeg studies in temporal lobe epilepsy. Epilepsia 1999;40(11):1587–92.

Marsh ED, Peltzer B, Brown III MW, Wusthoff C, Storm Jr PB, Litt B, et al. Interictal eeg spikes identify the region of electrographic seizure onset in some, but not all, pediatric epilepsy patients. Epilepsia 2010;51(4):592–601.

Mitra P. Observed brain dynamics. Oxford University Press; 2007.

Morgan RJ, Soltesz I. Nonrandom connectivity of the epileptic dentate gyrus predicts a major role for neuronal hubs in seizures. Proc Natl Acad Sci 2008;105(16):6179–84.

Nayel MH, Awad IA, Luders H. Extent of mesiobasal resection determines outcome after temporal lobectomy for intractable complex partial seizures. Neurosurgery 1991;29(1):55–61.

Newman ME. Scientific collaboration networks. ii. Shortest paths, weighted networks, and centrality. Phys Rev E 2001;64(1):016132.

Newman ME. Modularity and community structure in networks. Proc Natl Acad Sci 2006;103(23):8577–82.

Newman ME, Girvan M. Finding and evaluating community structure in networks. Phys Rev E 2004;69(2):026113.

Opsahl T, Agneessens F, Skvoretz J. Node centrality in weighted networks: generalizing degree and shortest paths. Soc Networks 2010;32(3):245–51.

Paolicchi JM, Jayakar P, Dean P, Yaylali I, Morrison G, Prats A, et al. Predictors of outcome in pediatric epilepsy surgery. Neurology 2000;54(3):642–7.

Rubinov M, Sporns O. Complex network measures of brain connectivity: uses and interpretations. NeuroImage 2010;52(3):1059–69. https://doi.org/10.1016/j.neuroimage.2009.10.003. ISSN 1095-9572.

Sabolek HR, Swiercz WB, Lillis KP, Cash SS, Huberfeld G, Zhao G, et al. A candidate mechanism underlying the variance of interictal spike propagation. J Neurosci 2012;32(9):3009–21.

Sammaritano M, Gigli GL, Gotman J. Interictal spiking during wakefulness and sleep and the localization of foci in temporal lobe epilepsy. Neurology 1991;41(2 Part 1):290.

Sarzynska M, Leicht EA, Chowell G, Porter MA. Null models for community detection in spatially embedded, temporal networks. J Complex Netw 2015;4(3):363–406.

Staba RJ, Wilson CL, Bragin A, Fried I, Engel J. Sleep states differentiate single neuron activity recorded from human epileptic hippocampus, entorhinal cortex, and subiculum. J Neurosci 2002;22(13):5694–704.

Steriade M, Contreras D, Amzica F. Synchronized sleep oscillations and their paroxysmal developments. Trends Neurosci 1994;17(5):201–7.

Tomlinson SB, Bermudez C, Conley C, Brown MW, Porter BE, Marsh ED. Spatiotemporal mapping of interictal spike propagation: a novel methodology applied to pediatric intracranial eeg recordings. Front Neurol 2016;7:229.

Trotta MS, Cocjin J, Whitehead E, Damera S, Wittig JH, Saad ZS, et al. Surface based electrode localization and standardized regions of interest for intracranial eeg. Hum Brain Mapp 2017;39:709–21.

Van Mierlo P, Carrette E, Hallez H, Vonck K, Van Roost D, Boon P, et al. Accurate epileptogenic focus localization through time-variant functional connectivity analysis of intracranial electroencephalographic signals. Neuroimage 2011;56 (3):1122–33.

Varotto G, Tassi L, Franceschetti S, Spreafico R, Panzica F. Epileptogenic networks of type ii focal cortical dysplasia: a stereo-eeg study. Neuroimage 2012;61 (3):591–8.

Wang S, Wang IZ, Bulacio JC, Mosher JC, Gonzalez-Martinez J, Alexopoulos AV, et al. Ripple classification helps to localize the seizure-onset zone in neocortical epilepsy. Epilepsia 2013;54(2):370–6.

Wendling F, Bartolomei F, Senhadji L. Spatial analysis of intracerebral electroencephalographic signals in the time and frequency domain: identification of epileptogenic networks in partial epilepsy. Philos Trans R Soc Lond A 2009;367(1887):297–316.

Wilke C, Van Drongelen W, Kohrman M, He B. Neocortical seizure foci localization by means of a directed transfer function method. Epilepsia 2010;51(4):564–72.

Wilke C, Worrell G, He B. Graph analysis of epileptogenic networks in human partial epilepsy. Epilepsia 2011;52(1):84–93.

Wyllie E, Luders H, Morris HH, Lesser RP, Dinner DS, Hahn J, et al. Clinical outcome after complete or partial cortical resection for intractable epilepsy. Neurology 1987;37(10):1634–41.